Cancer Research

Hypoxia-Induced Gene Expression in Chemoradioresistant Cervical Cancer Revealed by Dynamic Contrast-Enhanced MRI

Cathinka Halle[1], Erlend Andersen[2], Malin Lando[1], Eva-Katrine Aarnes[1], Grete Hasvold[1], Marit Holden[6], Randi G. Syljuåsen[1], Kolbein Sundfør[3], Gunnar B. Kristensen[3,4], Ruth Holm[5], Eirik Malinen[2], and Heidi Lyng[1]

Abstract

Knowledge of the molecular background of functional magnetic resonance (MR) images is required to fully exploit their potential in cancer management. We explored the prognostic impact of dynamic contrast-enhanced MR imaging (DCE-MRI) parameters in cervical cancer combined with global gene expression data to reveal their underlying molecular phenotype and construct a representative gene signature for the relevant parameter. On the basis of 78 patients with cervical cancer subjected to curative chemoradiotherapy, we identified the prognostic DCE-MRI parameter A_{Brix} by pharmacokinetic analysis of pretreatment images based on the Brix model, in which tumors with low A_{Brix} appeared to be most aggressive. Gene set analysis of 46 tumors with pairwise DCE-MRI and gene expression data showed a significant correlation between A_{Brix} and the hypoxia gene sets, whereas gene sets related to other tumor phenotypes were not significant. Hypoxia gene sets specific for cervical cancer created in cell culture experiments, including both targets of the hypoxia inducible factor (HIF1α) and the unfolded protein response, were the most significant. In the remaining 32 tumors, low A_{Brix} was associated with upregulation of HIF1α protein expression, as assessed by immunohistochemistry, consistent with increased hypoxia. On the basis of the hypoxia gene sets, a signature of 31 genes that were upregulated in tumors with low A_{Brix} was constructed. This DCE-MRI hypoxia gene signature showed prognostic impact in an independent validation cohort of 109 patients. Our findings reveal the molecular basis of an aggressive hypoxic phenotype and suggest the use of DCE-MRI to noninvasively identify patients with hypoxia-related chemoradioresistance. *Cancer Res; 72(20); 5285–95. ©2012 AACR.*

Introduction

Magnetic resonance imaging (MRI) is an indispensable tool in cancer management, and is widely used for staging, treatment planning, and response monitoring (1). Functional MRI, such as dynamic contrast-enhanced (DCE)-MRI, provides biologic information related to tumor physiology (2). There is a growing interest to use dynamic contrast enhanced MR imaging (DCE-MRI) to improve patient care by integrating anatomical and functional features (3). Locally advanced cervical cancer is one of the malignant diseases for which the inclusion of DCE-MRI could be helpful in clinical decision-making (1). Radiotherapy, often combined with cisplatin, is the primary treatment of choice and is challenging because of the risk of severe radiotoxicity in critical organs within the pelvis (4). Studies have suggested that DCE-MRI of cervical cancer depicts functional features associated with progressive disease (5–8). The ability of the technique to visualize tumor aggressiveness has, however, hardly been used, partly because the biologic meaning of the images is not completely understood (9).

DCE-MRI measures the temporal uptake pattern of a contrast agent in the tumor. When gadopentetate dimeglumine (Gd-DTPA) is used as contrast agent, the uptake mostly depends on the blood perfusion and the volume of the extracellular space (2). Biologic information can be extracted from the images by pharmacokinetic analysis of the uptake curves, where the Tofts and Brix models are most commonly applied (10). The Brix model has been recommended because the concentration of contrast agent in blood, that is, the arterial input function, is not needed in the calculations, making it particularly attractive for use in clinical routines (9). To fully exploit the potential of such models, a robust DCE-MRI biomarker should be identified and its molecular background clarified. Global gene expression profiles provide a detailed picture of the transcriptional program in tumors and thereby insight into the molecular phenotype. A few studies combining imaging and gene expression data have so far emerged, conveying results that encourage further work using this approach (11, 12).

In this study, we aimed to clarify the prognostic potential of the DCE-MRI Brix model parameters in patients with cervical cancer subjected to curative chemoradiotherapy and explore

Authors' Affiliations: Departments of [1]Radiation Biology, [2]Medical Physics, [3]Gynecologic Oncology; [4]Institute for Medical Informatics; [5]Department of Pathology, The Norwegian Radium Hospital; and [6]Norwegian Computing Center, Oslo, Norway

Note: Supplementary data for this article are available at Cancer Research Online (http://cancerres.aacrjournals.org/).

Corresponding Author: Heidi Lyng, Department of Radiation Biology, The Norwegian Radium Hospital, Nydalen, 0424 Oslo, Norway. Phone: 47-2278-1478; Fax: 47-2278-1495; E-mail: heidi.lyng@rr-research.no

doi: 10.1158/0008-5472.CAN-12-1085

their molecular background by use of gene expression profiles. In a cohort of 78 patients, we carried out pharmacokinetic analyses of pretreatment DCE-MR images and generated parameter histograms of each tumor to account for the intratumor heterogeneity in physiologic conditions. For the most prognostic parameter, the percentiles showing the strongest association with survival were used to extract a DCE-MRI parameter that was combined with global gene expression data. We further searched for a gene signature that reflected this parameter and contained molecular information about the potential aggressive phenotype visualized in the images. Our study shows the feasibility of this approach to decipher the molecular background of functional images and to identify a gene signature that reflects an aggressive cancer phenotype.

Materials and Methods

Patients and tumor specimens

A total of 187 patients with cervical carcinoma, prospectively recruited to our chemoradiotherapy protocol at the Norwegian Radium Hospital from 2001 to 2006, were included (Supplementary Table S1). Pretreatment DCE-MRI images suitable for analysis were available for 78 patients (DCE-MRI cohort). Three additional patients in our previous descriptive DCE-MRI study (7) were excluded because of unsatisfactorily fitting of the pharmacokinetic model. The remaining 109 patients served as an independent validation cohort based on their gene expression profiles. Possible pathologic lymph nodes in the pelvis at the time of diagnosis were evaluated by MRI, according to the response evaluation criteria in solid tumors version 1.1 (13). All patients were treated with external radiation of 50 Gy to the tumor, parametria, and adjacent pelvic wall, and with 45 Gy to the remaining part of the pelvic region. This was followed by brachytherapy of 21 Gy to point A. Adjuvant cisplatin (40 mg/m^2) was given weekly during the course of external radiation. Follow up consisted of clinical examinations, and when symptoms of relapse were seen, MR imaging of pelvis and retroperitoneum as well as X-ray of thorax were carried out. Relapse (progressive disease) was classified as locoregional (regression within the irradiated field), distant, or both.

One to 4 tumor biopsies, approximately $5 \times 5 \times 5$ mm in size, were taken before the start of therapy, immediately snap frozen, stored at -80°C, and used for gene expression analysis. A separate specimen was fixed in 4% buffered formalin, paraffin-embedded, and used for immunohistochemistry. The study was approved by the regional committee of medical research ethics in southern Norway, and written informed consent was achieved from all patients.

DCE-MRI

A 1.5 T Signa Horizon LX tomography (GE Medical Systems) with a pelvic-phased array coil was used for MRI. Standard T1- and T2-weigthed imaging was carried out in addition to DCE-MRI. To record the DCE-MRI series, an axial T1-weighted fast spoiled gradient recalled sequence was used (7). Gd-DTPA (0.1 mmoL/kg body weight; Magnevist; Schering) was administered as a fast bolus injection. The sequence of DCE-MRI included 14 image series during a time period of 5 minutes, of which 1 series was recorded before the bolus injection and 13 after. The temporal resolution was 15 seconds for the first 11 image series and 1 minute for the remaining 2 series.

Image analysis

The tumor outline was assessed in axial T2-weighted images by an experienced radiologist, and transferred to the DCE series by coordinate mapping (Fig. 1A; ref. 7). The relative signal increase (RSI) was used as measure of the uptake of contrast agent and was calculated for each tumor voxel and time point, using the relation:

$$\mathrm{RSI}(t) = \frac{S(t) - S(0)}{S(0)} \qquad \text{(a)}$$

where $S(t)$ is the signal intensity at time t, and $S(0)$ is the signal intensity in the precontrast images. Using Levenberg–Marquardt least squares minimization (14), the Brix model (10) was fitted to the uptake curve of each tumor voxel, using the relation:

$$\mathrm{RSI}(t) = A_{\mathrm{Brix}} \cdot \frac{k_{\mathrm{ep}}}{k_{\mathrm{el}} - k_{\mathrm{ep}}} \cdot \left(e^{-k_{\mathrm{ep}}t} - e^{-k_{\mathrm{el}}t}\right) \qquad \text{(b)}$$

where A_{Brix} is the amplitude, k_{ep} the transfer rate of tracer from tissue to plasma, and k_{el} the clearance rate of the tracer from plasma. The parameters were allowed to vary freely in the fitting, except for the constraints A_{Brix}, k_{ep}, $k_{\mathrm{el}} \geq 0$. Parameter maps were created to visualize the distribution of parameter values within the tumors (Fig. 1B and data not shown). To investigate the correlation between the parameters and clinical outcome, a percentile screening method presented previously (7) was applied. In brief, for each tumor, a parameter histogram was generated and percentile values from the 1st to the 100th percentile were calculated (Fig. 1B and data not shown). On the basis of their nth percentile value, the patients were separated into 2 equally sized groups, and log-rank tests were employed to assess whether the risk of relapse differed significantly between the 2 groups. The relative risk (RR) and its 95% confidence interval (CI) were plotted as a function of percentile, and for A_{Brix}, the prognostic parameter was calculated as the mean value over the percentile interval with the most significant RR; that is, with the strongest association to outcome (Fig. 1C). For k_{ep} and k_{el}, the associations with survival were nonsignificant or significant only within a small percentile interval (Supplementary Fig. S1), and they were therefore not included in further analyses.

Cell lines and hypoxia treatment

The HeLa, SiHa, and CaSki cervical cancer cell lines from American Type Culture Collection were used to generate cervical cancer–specific gene sets of hypoxia responsive genes. The cells were identity tested before the experiments by short tandem repeat (STR) profiling using Powerplex 16 (Promega), which amplifies 15 STR loci and amelogenin for gender identification: Penta E, D18S51, D21S11, TH01, D3S1358, F GA,

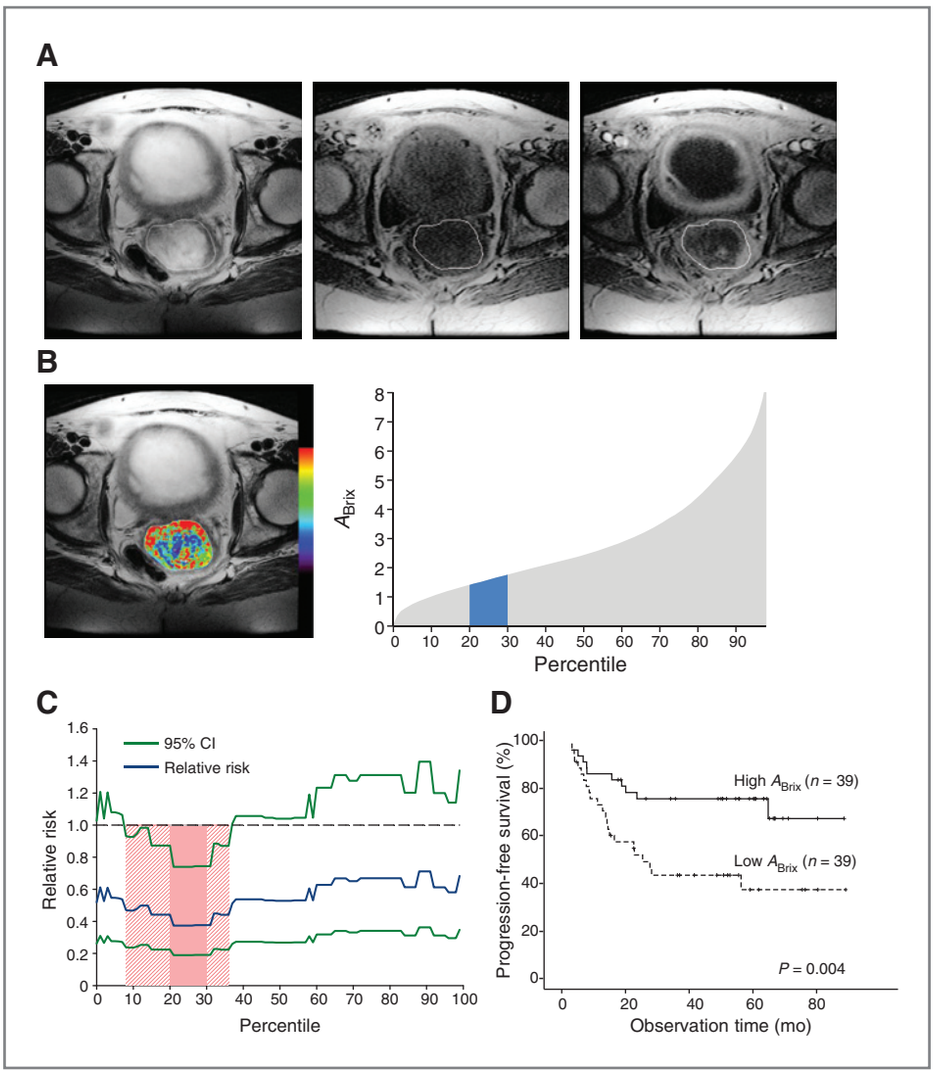

Figure 1. Identification of a prognostic A_{Brix} DCE-MRI parameter. A, T2-weighted (left), T1-weighted precontrast (middle), and T1-weighted postcontrast (right) MR image of a cervical cancer patient with the tumor delineated. B, tumor A_{Brix} map superimposed on a T2-weighted MR image (left) and the corresponding cumulative A_{Brix} histogram with the 20th to 30th percentiles indicated in blue (right) of the patient in A. Purple color in the A_{Brix} map represents A_{Brix} values of 0; red represents values of $\geq$5.0. C, relative risk (blue line) and 95% confidence interval (CI; green lines) from log-rank tests, comparing progression-free survival of 2 equally sized patient groups for each of 100 percentiles of the tumor A_{Brix} histograms, plotted against percentile (left). The significant 20th to 30th and 8th to 36th percentiles are indicated with a red bar and hatches, respectively. The upper 95% CI limit for significance is marked (dotted line). D, Kaplan-Meier curves for progression-free survival of patients with low (below median) and high (above median) A_{Brix}. A_{Brix} was calculated from each tumor histogram as the mean value over the 20th to 30th percentiles. P-value from log-rank test and number of patients are indicated.

TPOX, D8S1179, vWA, Amelogenin, Penta D, CSF1PO, D16S539, D7S820, D13S317, and D5S818.

The cells were incubated in Dulbecco's modified Eagle medium with GlutaMAX supplemented with 10% fetal calf serum and 100 U/mL penicillin/streptomycin (Gibco) under a 5% CO_2 atmosphere at 37°C. Cells were plated out in plastic dishes (3×10^5 cells for 6 cm dishes, 9×10^5 for 10 cm dishes) 24 hours before exposure to hypoxic (0.2% O_2, 5% CO_2) or normoxic (95% air, 5% Co_2) conditions for 24 hours at 37°C. The hypoxia treatment was carried out in an Invivo$_2$200 chamber (Ruskinn Technology Ltd.) with accurate O_2 and CO_2 controls. The treatment conditions of 24 hours with 0.2% O_2 were selected to mimic conditions with prolonged hypoxia and ensure a response by HIF1α and possibly by the unfolded protein response (UPR; ref. 15).

The cell-cycle distribution was analyzed on an LSR II flow cytometer (Becton Dickinson) after fixation in 70% ethanol and staining with 1.5 μg/mL Hoechst 33258. Western blots were carried out by lysing cells with 10 mmol/L Tris HCl lysis buffer (pH 7.5) containing 2% SDS and 100 μmol/L Na_3VO_4. The proteins were separated by 8% Tris-HEPES-SDS polyacrylamide gels (Pierce Biotechnology), blotted on a PVDF membrane and stained with the monoclonal mouse HIF1α antibody clone 54 (1:800, no. 610958; BD Transduction Laboratories) and donkey antimouse secondary antibody (715-001-003; Jackson ImmunoResearch Laboratories, Inc.).

Gene expression analysis

Gene expression profiling of 155 patients (46 in the DCE-MRI cohort, 109 in the validation cohort) as well as normoxia- and hypoxia-treated cell lines was carried out using the Illumina bead arrays human WG-6 v3 (Illumina Inc.) with 48803 transcripts (16). In brief, total RNA was isolated from the frozen tumor specimens using Trizol reagent (Invitrogen) and from the cell lines using RNeasy MiniKit (Quiagen). cRNA was synthesized, labeled, and hybridized to the arrays. Signal extraction and quantile normalization were carried out by the software provided by the manufacturer (Illumina Inc.).

Log-transformed data were used in the analyses. All clinical specimens had more than 50% (median 70%) tumor cells in hematoxilin and eosin stained sections derived from the central part of the biopsy. RNA from different biopsies of the same tumor was pooled. The Illumina data have been deposited to the GEO repository (GSE36562).

Computational analysis of gene expression profiles

To explore biologic processes associated with A_{Brix}, a list of genes was generated from the expression profiles of 46 DCE-MRI patients, based on the Spearman rank correlation between gene expression and A_{Brix}. A cut off *P*-value of 0.05 was used to achieve an appropriate number of genes for further analysis. The gene ontology (GO) categories of the correlating genes were compared with those of all genes on the array using the master-target procedure with the Fisher's exact test in the eGOn software, where a multiple testing algorithm was used to control the false discovery rate (FDR; ref. 17). Furthermore, the gene set analysis tool Significance Analysis of Microarrays for Gene Sets (SAM-GS), which is based on the moderated *t*-statistic in SAM (18) and with the same multiple testing procedure as above to control FDR, was used for a supervised analysis on 16 gene sets comprising biologic processes that were significant in the GO analysis. Seven of the gene sets have been published previously (19–24), 5 sets were based on the Kyoto Encyclopedia of Genes and Genomes (KEGG) and Reactome pathway databases and 4 sets were generated from the gene expression data of the hypoxia-treated cervical cancer cell lines (Supplementary Methods S1). Since multiple gene symbols may exist for the same genes, the symbols in the various gene sets were altered to match those in our Illumina data set and only genes that could be found in our data set were included in the final gene sets (Supplementary Methods S2). For the gene set analysis, the patients were classified into a low A_{Brix} group or a high A_{Brix} group, based on the median value of A_{Brix} in the 78 DCE-MRI patients. The Illumina data file was reduced to one probe per gene by selecting the probe with the greatest average difference between the low and high A_{Brix} groups.

Immunohistochemistry

Immunohistochemistry (IHC) was carried out on 32 selected tumors with the monoclonal mouse HIF1α antibody clone 54 (1:25, no. 610958; BD Transduction Laboratories), binding the amino acid 610 to 727 on the HIF1α protein. The tissue sections (4 μm) were stained using the Dako EnVisionTM Flex+ System (K8012; Dako). For antigen retrieval, the PT-Link (Dako) and EnVisionTM Flex target retrieval solution at a high pH were used, and the sections were incubated with the HIF1α antibody for 30 minutes. A cervical tumor known to express HIF1α was used as a positive control, whereas as a negative control the antibody was substituted with mouse myeloma protein of the same concentration and subclass as the HIF1α antibody. Nuclear staining was scored on the basis of the percentage of positive tumor cells: 0, 0%; 1, 1% to 10%; 2, 11% to 25%; 3, 26% to 50%; 4, 51% to 75%; and 5, >75%. The cytoplasmic staining was generally weak or absent, and was therefore not quantified. The scoring was carried out by an experienced scientist at the Department of Pathology (R.H.) who was blinded to the DCE-MRI data.

Table 1. Gene sets associated with A_{Brix}

Gene set[a]	No. of genes	*P*	Adj. *P*[b]
Hypoxia cervical up ×3	79	0.009	0.122
Hypoxia cervical up and literature	286	0.018	0.122
MENSE_HYPOXIA_UP (22)[c]	95	0.025	0.122
WINTER_HYPOXIA_UP (24)[c]	91	0.032	0.122
REACTOME_CELL_CYCLE_CHECKPOINTS	110	0.038	0.122
KEGG_NON_HOMOLOGOUS_END_JOINING	13	0.052	0.138
Hypoxia cervical down and literature	183	0.068	0.156
KEGG_HOMOLOGOUS_RECOMBINATION	27	0.082	0.163
STARMANS_WOUND_SIGNATURE (23)	413	0.093	0.166
CHIANG_LIVER_CANCER_SUBCLASS_PROLIFERATION_UP (20)[c]	136	0.127	0.202
STARMANS_PROLIFERATION_SIGNATURE (23)	104	0.172	0.239
Hypoxia cervical down ×3	10	0.179	0.239
KEGG_PROTEIN_PROCESSING_IN_ER	162	0.258	0.296
ISHIGAMI_RADIATION_RESISTANCE (21)	25	0.259	0.296
KEGG_BASE_EXCISION_REPAIR	32	0.527	0.562
AMUNDSON_GAMMA_RADIATION_RESISTANCE (19)[c]	17	0.585	0.585

NOTE: Gene expression profiles of tumors with high (above median) and low (below median) A_{Brix} were compared.

[a]Gene sets in bold were created from cervical cancer cell lines in the present work, whereas the remaining gene sets were taken from the literature or from the Reactome, KEGG, or Molecular Signatures databases. References to the relevant literature are listed.

[b]The *P* values were adjusted for multiple testing.

[c]Obtained from the Molecular Signatures Database (MSigDB) v3.0.

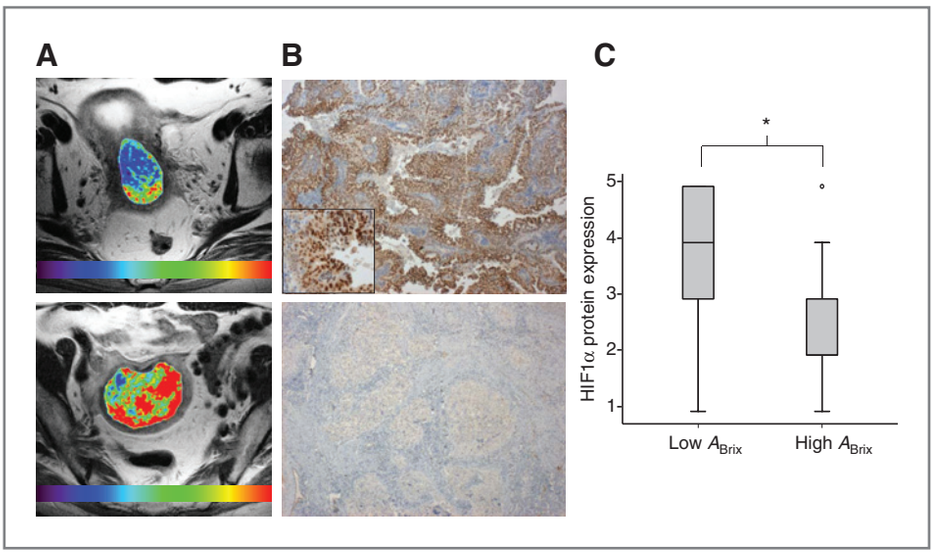

Figure 2. Association between A_{Brix} and HIF1α protein expression. A, tumor A_{Brix} maps superimposed on T2-weighted MR images of 2 different patients with cervical cancer. Purple color represents A_{Brix} values of 0 and red represents values of ≥5.0. B, representative sections showing HIF1α protein expression of the tumors in A. Inset shows nuclear HIF1α expression. Original magnification, ×4; inset image, ×10. A and B, a tumor with low (below median, upper) and high (above median, lower) A_{Brix}, as calculated from the tumor histogram as the mean value over the 20th to 30th percentiles. C, box plot (median, first, and third quartile) showing nuclear HIF1α protein expression in tumors with low ($n = 17$) and high ($n = 15$) A_{Brix}, respectively. The whiskers extend to the farthest points that are not outliers. The patients are grouped on the basis of the median A_{Brix} in the 78 DCE-MRI patients. *, $P < 0.01$ (Mann–Whitney U test).

Statistics

Mann–Whitney U test was used for comparison of the protein expression level of HIF1α in the patient group with low A_{Brix} versus high A_{Brix}. In the survival analyses, the endpoint was progression-free survival, where the time from diagnosis to cancer-related death or to the first event of relapse was used, or locoregional control, which was defined as control within the irradiated pelvic region including lymph nodes. Thirteen patients died of causes not related to cancer and were censored. Cox proportional hazard analysis was used to evaluate the prognostic value of various parameters with respect to progression-free survival and locoregional control. Kaplan-Meier curves were compared using log-rank test. P-values <0.05 were considered significant.

Results

Patients with low A_{Brix} have a poor outcome after chemoradiotherapy

The prognostic potential of the DCE-MRI A_{Brix} parameter was explored by evaluating the relative risk of all percentiles in the A_{Brix} histograms, which enabled us to judge different parts of the histograms separately and identify the one with the strongest relationship to outcome (7). The lower A_{Brix} values harbored the strongest prognostic information, and a broad range from the 6th to 59th percentile was associated with progression-free survival at a significance level below 0.08 (Fig. 1C), indicating considerable robustness in the A_{Brix} parameter (7). The interval from the 8th to 36th percentile had a significance level below 0.05, whereas the 20th to 30th percentiles were the most significant ones (RR < 0.44, $P < 0.018$; Fig. 1C). The mean of A_{Brix} values over the 20th to 30th percentiles was therefore used as the representative A_{Brix} imaging parameter. This A_{Brix} parameter varied considerably among the patients, ranging from 0.59 to 3.21, with a median of 1.50. Patients with an A_{Brix} below the median showed a poor outcome compared with the others, and the probability of survival differed with more than 30% at 5 years follow-up between the 2 groups ($P = 0.004$; Fig. 1D).

Low A_{Brix} associates with upregulation of hypoxia response genes and HIF1α protein

To examine whether the differences in A_{Brix} among the tumors were reflected in the transcriptional program of specific biologic processes, we combined the gene expression profiles of 46 tumors with the DCE-MRI data. We first used an unsupervised GO analysis to obtain a general picture of the biology in low A_{Brix} tumors, where the genes with the highest correlation between expression and A_{Brix} were included. Four major significant processes were identified; metabolism, cell cycle, cellular component organization and biosynthesis, and response to DNA damage stimulus (Supplementary Table S2). On the basis of these results, a supervised gene set analysis was carried out on all genes on the array to more specifically investigate phenotypes that could be reflected in A_{Brix}. The correlation between A_{Brix} and the categories metabolism, cell cycle, and cellular component organization and biosynthesis could indicate both altered proliferation and presence of hypoxia. Published gene sets associated with these phenotypes were therefore included (20, 22–24). To cover the process response to DNA damage stimulus, published gene sets representing intrinsic radioresistance were used (19, 21) as well as the KEGG DNA repair pathways for nonhomologous end-

Table 2. The DCE-MRI hypoxia gene signature

Probe ID[a]	Gene symbol[b,c]	Gene name	P^d	Corr[d]
	Metabolism			
2470341	**ALDOA**	Aldolase A, fructose-bisphosphate	0.038	−0.307
1990491	AK2	Adenylate kinase 2	0.038	−0.306
160148	AK3L1	Adenylate kinase 4	0.010	−0.378
2640386	B3GNT4	UDP-GlcNAc:betaGal beta-1,3-N-acetylglucosaminyltransferase 4	0.004	−0.416
1170338	SCARB1	Scavenger receptor class B, member 1	0.003	−0.314
4640041	CLK3	CDC-like kinase 3	0.046	−0.295
7380634	C20ORF20	Chromosome 20 open reading frame 20	0.017	−0.350
630674	ECE2	Endothelin converting enzyme 2	0.017	−0.350
4780671	**ERO1L**	ERO1-like (S. cerevisiae)	0.019	−0.343
2640048	**GAPDH**	Glyceraldehydes-3-phosphate dehydrogenase	0.041	−0.302
6660601	**HMOX1**	Heme oxygenase (decycling) 1	0.024	−0.333
2100196	ISG15	ISG15 ubiquitin-like modifier	0.038	−0.308
7400653	**PFKFB4**	6-Phosphofructo-2-kinase/fructose-2,6-biphosphatase 4	0.035	−0.311
270408	**P4HA2**	Prolyl 4-hydroxylase, alpha polypeptide II	0.050	−0.291
2760427	PYGL	Phosphorylase, glycogen, liver	0.011	−0.371
6280632	RPL36A	Ribosomal protein L36a	0.041	−0.302
2190408	UPK1A	Uroplakin 1A	0.008	−0.383
	Cell cycle			
830619	DDIT3	DNA-damage–inducible transcript 3	0.004	−0.414
2760008	KCTD11	Potassium channel tetramerisation domain containing 11	0.022	−0.338
780524	PVR	Poliovirus receptor	0.047	−0.295
	Proliferation			
4390619	RHOC	Ras homolog gene family, member C	0.043	−0.299
1170170	**STC2**	Stanniocalcin 2	0.007	−0.390
	Other			
2100341	C14ORF2	Chromosome 14 open reading frame 2	0.030	−0.321
3460184	C19ORF53	Chromosome 19 open reading frame 53	0.017	−0.352
1980369	**C4ORF3**	Chromosome 4 open reading frame 3	0.049	−0.292
5900025	FGF11	Fibroblast growth factor 11	0.033	−0.315
1300603	SH3GL3	SH3-domain GRB2-like 3	0.038	−0.307
5690431	SNTA1	Syntrophin, alpha 1 (dystrophin-associated protein A1, 59 kDa, acidic component)	0.012	−0.366
3440070	SPAG7	Sperm associated antigen 7	0.011	−0.372
2970017	S100A2	S100 calcium binding protein A2	0.009	−0.381
3420671	TRAPPC1	Trafficking protein particle complex 1	0.008	−0.384

[a]Illumina probe ID.
[b]HUGO gene symbol.
[c]Genes in bold are known HIF1α targets and underlined genes are known to be involved in the unfolded protein response.
[d]Correlation coefficient (Corr) and *P* value in Spearman rank correlation analysis of A_{Brix} versus gene expression.

joining, homologous recombination, and base excision repair. The cell-cycle checkpoints pathway from Reactome was also included to represent both this process and the cell-cycle category. Moreover, the KEGG pathway for protein processing in endoplasmic reticulum (ER) was used to cover the metabolism category more thoroughly because the protein modification process was one of its significant subcategories. Finally, we included a published gene set associated with wound healing that has shown prognostic impact in several other tumor types (23).

The most significantly differentially expressed gene sets when comparing tumors with high (above median) and low (below median) A_{Brix} were those representing hypoxia ($P = 0.025$ and 0.032; Supplementary Table S3). The cell-cycle checkpoints pathway was also significant ($P = 0.038$), and a closer look at its genes revealed that several of those that were correlated with A_{Brix} are known to be activated under hypoxia, such as *ATR* and *CHEK2* (25). Thus, A_{Brix} seemed to be associated with the transcriptional program regulated under hypoxia.

The transcriptional hypoxia response has been shown to differ among tumor types (26). A cervical cancer–specific hypoxia gene set could possibly be more strongly associated with A_{Brix} than the gene sets used above and thus contain genes

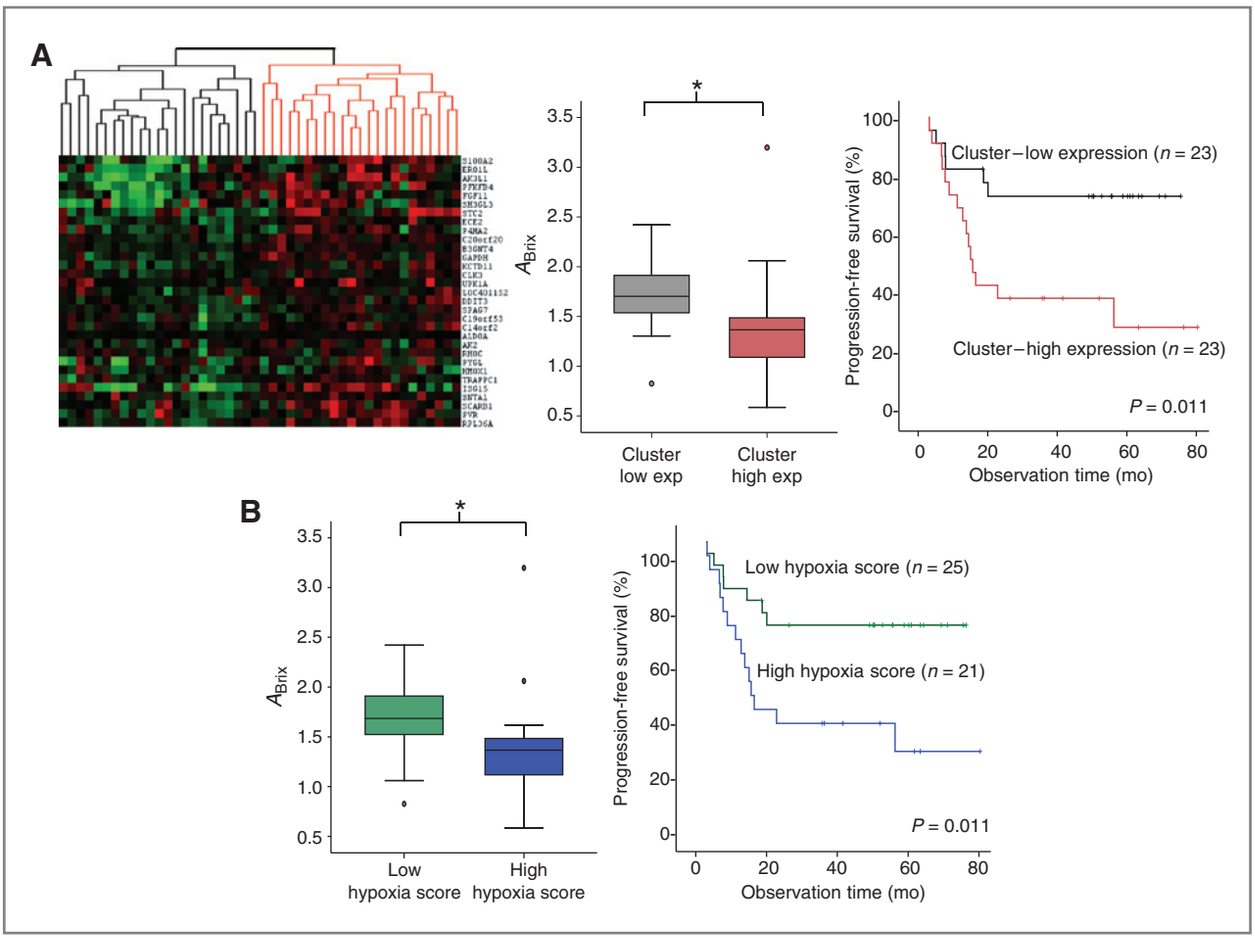

Figure 3. The DCE-MRI hypoxia gene signature in relation to A_{Brix} and clinical outcome. A, hierarchical clustering of the 46 cervical cancer patients with both DCE-MRI and gene expression data based on expression of the 31 genes in the DCE-MRI hypoxia gene signature (left). Box plot of A_{Brix} (middle) and Kaplan-Meier curves for progression-free survival (right) of patients in the low (black) and high (red) expression cluster. B, box plot of A_{Brix} (left) and Kaplan-Meier curves for progression-free survival (right) of patients with low (green) and high (blue) DCE-MRI hypoxia score. The box plots show median, first, and third quartile; the whiskers extend to the farthest points that are not outliers. $^*P < 0.01$ (Mann–Whitney U test). P values from log-rank test and number of patients are indicated in the Kaplan-Meier plots.

that would be important for the creation of a robust gene signature that reflected A_{Brix}. We therefore generated hypoxia gene sets based on the expression profiles of cervical cancer cells grown under hypoxia. HIF1α protein was upregulated in all 3 cell lines by the hypoxia treatment, whereas only minor changes were observed in the cell-cycle distributions (Supplementary Fig. S2A and S2B). Four different gene sets were generated from the hypoxia induced expression changes; genes upregulated in all 3 cell lines, genes upregulated in one of the cell lines and confirmed as hypoxia regulated by the literature, and correspondingly for the downregulated genes (Supplementary Methods S1 and S2). In the second round of gene set analysis, the cervical cancer–specific hypoxia gene sets with upregulated genes were found to be the most significant ones (Table 1). These results supported the suggestion of a correlation between A_{Brix} and hypoxia, and showed that the cervical cancer–specific gene sets could be useful in the construction of an A_{Brix} gene signature.

To confirm the above finding of a correlation between A_{Brix} and hypoxia, protein expression of HIF1α was assessed by immunohistochemistry in the 32 remaining DCE-MRI patients who had not been evaluated in the gene expression study. HIF1α was selected as hypoxia marker because a hypoxia-induced HIF1α response was observed in the cell lines (Supplementary Fig. S2B). The patients with low A_{Brix} had a significantly higher HIF1α expression compared with those with high A_{Brix} ($P = 0.004$; Fig. 2A–C). In accordance with this result, several of the HIF1α targets were upregulated in tumors with low A_{Brix} in the DCE-MRI patients used for gene expression analysis. We thus concluded that low A_{Brix} was associated with tumor hypoxia and upregulation of hypoxia response genes.

A_{Brix} reflects a hypoxia gene signature with prognostic impact in an independent cohort

To construct a DCE-MRI signature with the most important genes reflected by A_{Brix}, we selected the 4 significant hypoxia

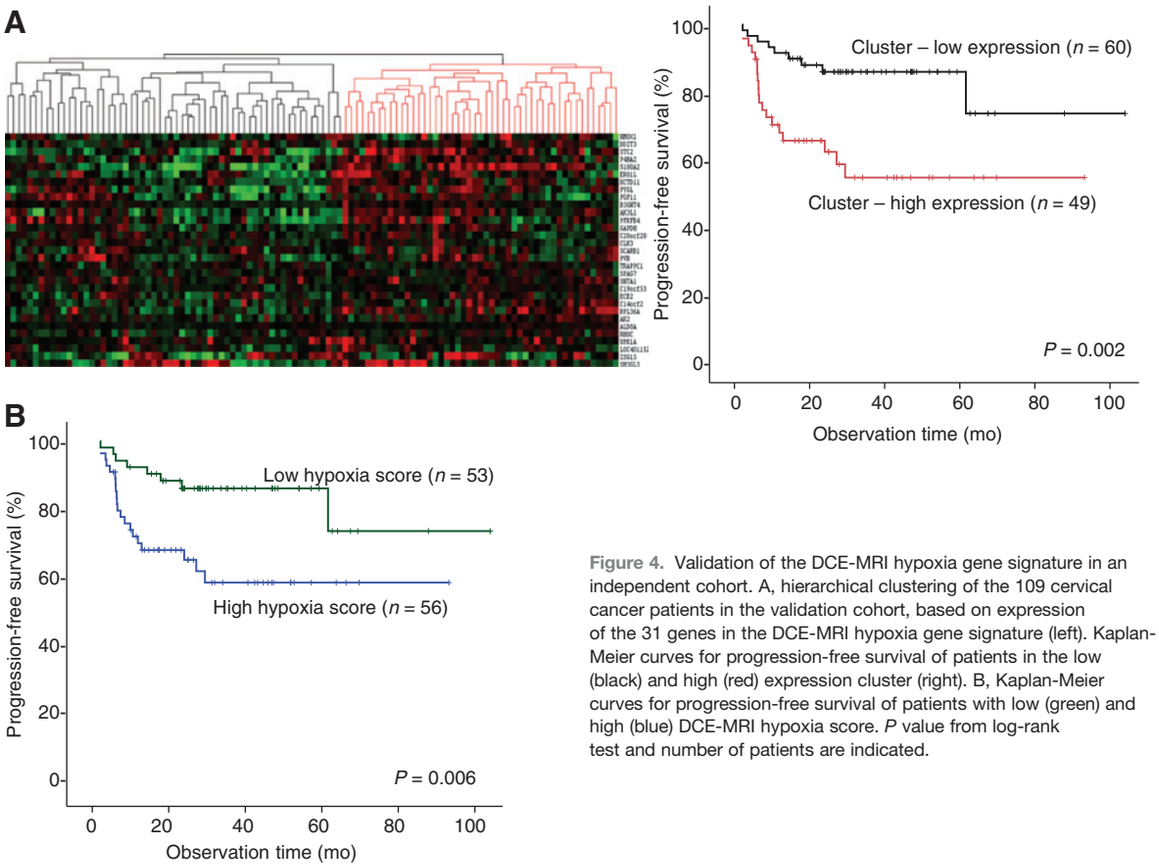

Figure 4. Validation of the DCE-MRI hypoxia gene signature in an independent cohort. A, hierarchical clustering of the 109 cervical cancer patients in the validation cohort, based on expression of the 31 genes in the DCE-MRI hypoxia gene signature (left). Kaplan-Meier curves for progression-free survival of patients in the low (black) and high (red) expression cluster (right). B, Kaplan-Meier curves for progression-free survival of patients with low (green) and high (blue) DCE-MRI hypoxia score. *P* value from log-rank test and number of patients are indicated.

gene sets (Table 1), and extracted the 31 genes with a negative correlation between the gene expression and A_{Brix}; that is, the genes that were upregulated in tumors with low A_{Brix}. Most of these 31 genes are known to participate in biologic processes affected by hypoxia, such as energy metabolism, cell cycle, and proliferation, including HIF1α targets such as *ALDOA*, *STC2*, and *HMOX1* (27–29), and genes involved in the UPR (*DDIT3*, *STC2*, *ERO1L*, and *AK2*; refs. 30–32; Table 2), suggesting that several parts of the hypoxia induced transcriptional program were reflected by A_{Brix}.

To ensure that the signature sufficiently represented the A_{Brix} parameter, we carried out unsupervised clustering of the 46 DCE-MRI patients based on the expressions of the 31 genes. Clustering showed 2 groups with different outcome, for which the one with high expression of hypoxia responsive genes had low A_{Brix} ($P < 0.001$) and poor outcome ($P = 0.011$) as compared with the other (Fig. 3A). We further calculated a hypoxia score for each tumor by averaging the median centered expression levels for the 31 genes, as described (26). In line with the above results, patients with a high hypoxia score had low A_{Brix} ($P < 0.001$) and poor outcome ($P = 0.011$) compared with the others (Fig. 3B). The DCE-MRI hypoxia gene signature therefore seemed to satisfactorily represent the A_{Brix} parameter, including its relationship to clinical outcome.

The prognostic impact of the gene signature was further validated in an independent cohort of 109 patients with cervical cancer. In this validation set, the patients who clustered together because of high expression of the genes in the signature had a significantly worse outcome than the remaining patients ($P = 0.002$; Fig. 4A). When assessing the hypoxia score in this cohort, the patients with a high score had a poor outcome compared with those with a low score ($P = 0.006$; Fig. 4B). The prognostic value of the signature was therefore confirmed. To assess the importance of the signature in comparison with existing clinical markers, the patients from the DCE-MRI cohort and the validation cohort were merged, and a multivariate Cox analysis was carried out on the resulting group of 155 patients. The hypoxia score emerged as a prognostic factor independent of lymph node status, FIGO stage, and tumor volume for both progression-free survival and locoregional control (Table 3).

Discussion

By integrating DCE-MRI and global gene expression data of cervical cancers, we found that the images reflect a transcriptional program regulated under hypoxia. This program included a gene signature with prognostic impact in an independent validation cohort, thus pointing to hypoxia-regulated

Table 3. Cox regression analysis of the hypoxia score and clinical variables

	Univariate analysis			Multivariate analysis		
Factor	***P***	**Relative Risk**	**95% CI**	***P***	**Relative Risk**	**95% CI**
Progression-free survival						
Lymph node status	0.007	2.20	1.24–3.89	N.S.	–	–
Tumor volume[a]	0.001	3.33	1.64–6.72	(0.069)	2.02	0.96–4.29
FIGO stage[b]	<0.001	3.40	1.93–5.97	0.001	2.81	1.52–5.20
Hypoxia score[c]	0.001	2.90	1.57–5.33	0.006	2.50	1.29–4.84
Locoregional control						
Lymph node status	0.120	2.27	0.81–6.38	–	–	–
Tumor volume[a]	0.102	2.60	0.83–8.20	–	–	–
FIGO stage[b]	0.080	2.48	0.89–6.86	(0.056)	2.70	0.97–7.50
Hypoxia score[c]	0.033	3.48	1.11–11.0	0.026	3.71	1.17–11.8

NOTE: The analysis was carried out on 155 patients, including both the DCE-MRI cohort and the validation cohort.
Abbreviations: FIGO, Federation International de Gynecologie et d'Obstetrique; N.S., nonsignificant.
[a]Tumor size was divided into 2 groups on the basis of the median volume of 43.8 cm^3.
[b]FIGO stage was divided into 2 groups: 1b–2b and 3a–4a.
[c]The hypoxia score was divided into 2 groups, based on values <0 and >0.

pathways that may promote cervical cancer aggressiveness. Tumor hypoxia is a known prognostic factor in many types of cancer, including cervical cancer (33), and would therefore be valuable to implement in clinical decision-making. Our work is the first to provide molecular insight into the DCE-MR images that could facilitate this strategy, encouraging the use of DCE-MRI as a tool to handle hypoxia-induced chemoradioresistance in cervical cancer.

Several evidences for a relationship between low A_{Brix} and tumor hypoxia were provided by our work. The hypoxia gene sets were significantly associated with A_{Brix}, and revealed upregulation of hypoxia response genes including HIF1α targets in tumors with low A_{Brix}. In line with this, tumors with low A_{Brix} had higher protein expression of HIF1α compared with those with high A_{Brix}. The results from the GO analysis were also in accordance with these conclusions, as the biologic processes metabolism, cell cycle, and DNA damage signaling, which were associated with A_{Brix}, are important targets for the hypoxia response (25, 28, 34). In particular, genes from the metabolism category encoding the glycolytic enzymes ALDOA, GAPDH, and PFK4B4 were found to be upregulated in tumors with low A_{Brix}, consistent with the increased glycolytic activity often seen in hypoxic tumors (28). Loncaster and colleagues (5) showed a relationship between A_{Brix} and oxygen tension in cervical tumors, as measured by Eppendorf pO_2 histography, supporting our conclusion.

Extraction of genes from the hypoxia gene sets that were upregulated in tumors with low A_{Brix} resulted in a DCE-MRI hypoxia gene signature that was associated with the clinical outcome, independent of clinical markers for progression-free survival. This suggests that the gene signature associated with A_{Brix} provides information of disease progression that is not covered by the conventional clinical parameters. In addition, the gene signature appeared as the most significant factor for locoregional control, indicating that hypoxia as measured by A_{Brix} could be a well-needed biomarker of local recurrence in cervical cancer. Furthermore, while previous studies have demonstrated the importance of hypoxia in resistance to radiotherapy (33), the strong prognostic impact of this hypoxia gene signature indicates that hypoxia also influences the effect of chemoradiotherapy in cervical cancer patients.

The use of global gene expression data enabled detailed insight into the transcriptional program reflected by A_{Brix}. The response to hypoxia occurs through different pathways, and may involve activation of HIFs, the UPR or ER stress response, and signaling through the mechanistic target of rapamycin (MTOR) kinase (32). Eight of the 31 genes in the DCE-MRI hypoxia gene signature are known HIF1α targets, namely *ALDOA*, *ERO1L*, *GAPDH*, *PFKFB4*, *P4HA2*, *C4orf3*, *HMOX1*, and *STC2* (27, 29, 32, 35, 36), although *SCARB1* is a target of HIF2 (the endothelial PAS domain protein 1, EPAS1; ref. 36). The protein encoded by one of the other genes, *RHOC*, is indirectly associated with HIF1α through its interaction with the von Hippel-Lindau tumor suppressor (VHL; ref. 37), which degrades HIF1α. In addition, *AK2, ERO1L, DDIT3* (also known as *CHOP*), and *STC2* have been found to be involved in the UPR (30–32, 38). It thus seems that processes associated with both HIF activation and UPR may be important in the hypoxic phenotype depicted by low A_{Brix}. The involvement of HIF activation was further supported by the high HIF1α protein expression in these tumors.

Current knowledge of how these genes influence cervical cancer progression is sparse. However, several of them or their encoded proteins, including *STC2*, *PFKFB4*, *RHOC*, *S100A2*, *HMOX1*, and *ISG15*, have been associated with poor prognosis in other cancer types (39–44). Moreover, upregulation of *ALDOA*, *GAPDH*, and *PFKFB4* suggest a high glycolytic activity, as mentioned above, which has been associated with aggressiveness (28). Furthermore, SCARB1, PVR, and RPL36A have been shown to promote rapid proliferation (45–47), and

AK4 may play a critical role in both cellular survival and proliferation during stress conditions such as hypoxia (48). Both *DDIT3* and *STC2* are targets of the activating transcription factor ATF4, which is induced by the eukaryotic translation initiation factor kinase EIF2AK3 (PERK) in response to hypoxia (31, 32, 49). STC2 has been shown to inhibit apoptosis and to induce proliferation and invasiveness in response to HIF1α or ER stress during hypoxia (27, 31, 50). DDIT3 on the other hand, is a proapoptotic protein, but was recently shown to protect tumor cells under hypoxia through the regulation of autophagy, proposing a role in the balance between autophagy and apoptosis (49). It may thus be speculated that the combined action of these 2 genes in tumors with low A_{Brix} promotes the adaption to hypoxia by inhibiting apoptosis and inducing autophagy. Taken together, these studies support a role of the signature genes in the development of an aggressive hypoxic phenotype.

Using DCE-MRI to assess hypoxia associated aggressiveness in cervical cancer is appealing because MRI is already in routine use for patient diagnosis at many hospitals (1). Furthermore, the use of noninvasive imaging to assess the molecular hypoxia phenotype could potentially reduce the need of invasive biopsy procedures and be carried out during the course of treatment for response evaluation. A_{Brix} seems to be a valuable DCE-MRI parameter for this purpose because of its strong correlation to outcome in our study. The robustness of the parameter, as suggested by the percentile analysis of A_{Brix} histograms, is supported by the cervical cancer study of Loncaster et al. (5), where A_{Brix} also had prognostic impact although the patient characteristics and MRI protocol differed from ours. In the present work, we have showed how noninvasive imaging by means of DCE-MRI and A_{Brix} assessment may visualize hypoxia and its molecular basis in chemoradioresistant tumors. Our results may have important clinical implications in that they suggest the use of DCE-MRI to identify patients with treatment-resistant tumors that may benefit from additional or alternative therapy targeting hypoxia.

Disclosure of Potential Conflicts of Interest

No potential conflicts of interest were disclosed.

Authors' Contributions

Conception and design: C. Halle, E. Malinen, H. Lyng
Development of methodology: E. Andersen, G. Hasvold, E. Malinen, H. Lyng
Acquisition of data (provided animals, acquired and managed patients, provided facilities, etc.): C. Halle, M. Lando, E.-K. Aarnes, G. Hasvold, R.G. Syljuåsen, K. Sundfør, G.B. Kristensen, E. Malinen, H. Lyng
Analysis and interpretation of data (e.g., statistical analysis, biostatistics, computational analysis): C. Halle, E. Andersen, M. Lando, G. Hasvold, M. Holden, R.G. Syljuåsen, R. Holm, E. Malinen, H. Lyng
Writing, review, and/or revision of the manuscript: C. Halle, M. Lando, E.-K. Aarnes, G. Hasvold, M. Holden, R.G. Syljuåsen, K. Sundfør, G.B. Kristensen, R. Holm, E. Malinen, H. Lyng
Administrative, technical, or material support (i.e., reporting or organizing data, constructing databases): E. Andersen, G.B. Kristensen, H. Lyng
Study supervision: H. Lyng

Grant Support

This work was supported by the Norwegian Cancer Society and the South-Eastern Norway Regional Health Authority.

The costs of publication of this article were defrayed in part by the payment of page charges. This article must therefore be hereby marked *advertisement* in accordance with 18 U.S.C. Section 1734 solely to indicate this fact.

Received March 21, 2012; revised June 26, 2012; accepted July 25, 2012; published OnlineFirst August 13, 2012.

References

1. Harry VN, Deans H, Ramage E, Parkin DE, Gilbert FJ. Magnetic resonance imaging in gynecological oncology. Int J Gynecol Cancer 2009;19:186–93.
2. Yankeelov TE, Gore JC. Dynamic contrast enhanced magnetic resonance imaging in oncology: theory, data acquisition, analysis, and examples. Curr Med Imaging Rev 2009;3:91–107.
3. Bayouth JE, Casavant TL, Graham MM, Sonka M, Muruganandham M, Buatti JM. Image-based biomarkers in clinical practice. Semin Radiat Oncol 2011;21:157–66.
4. Elliott SP, Malaeb BS. Long-term urinary adverse effects of pelvic radiotherapy. World J Urol 2011;29:35–41.
5. Loncaster JA, Carrington BM, Sykes JR, Jones AP, Todd SM, Cooper R, et al. Prediction of radiotherapy outcome using dynamic contrast enhanced MRI of carcinoma of the cervix. Int J Radiat Oncol Biol Phys 2002;54:759–67.
6. Yuh WT, Mayr NA, Jarjoura D, Wu D, Grecula JC, Lo SS, et al. Predicting control of primary tumor and survival by DCE MRI during early therapy in cervical cancer. Invest Radiol 2009;44: 343–50.
7. Andersen EK, Hole KH, Lund KV, Sundfor K, Kristensen GB, Lyng H, et al. Dynamic contrast-enhanced MRI of cervical cancers: temporal percentile screening of contrast enhancement identifies parameters for prediction of chemoradioresistance. Int J Radiat Oncol Biol Phys 2012;82:e485–92.
8. Donaldson SB, Buckley DL, O'Connor JP, Davidson SE, Carrington BM, Jones AP, et al. Enhancing fraction measured using dynamic contrast-enhanced MRI predicts disease-free survival in patients with carcinoma of the cervix. Br J Cancer 2010;102:23–6.
9. Zwick S, Brix G, Tofts PS, Strecker R, Kopp-Schneider A, Laue H, et al. Simulation-based comparison of two approaches frequently used for dynamic contrast-enhanced MRI. Eur Radiol 2010;20:432–42.
10. Tofts PS. Modeling tracer kinetics in dynamic Gd-DTPA MR imaging. J Magn Reson Imaging 1997;7:91–101.
11. Diehn M, Nardini C, Wang DS, McGovern S, Jayaraman M, Liang Y, et al. Identification of noninvasive imaging surrogates for brain tumor gene-expression modules. Proc Natl Acad Sci U S A 2008;105:5213–8.
12. Segal E, Sirlin CB, Ooi C, Adler AS, Gollub J, Chen X, et al. Decoding global gene expression programs in liver cancer by noninvasive imaging. Nat Biotechnol 2007;25:675–80.
13. van Persijn van Meerten EL, Gelderblom H, Bloem JL. RECIST revised: implications for the radiologist. A review article on the modified RECIST guideline. Eur Radiol 2010;20:1456–67.
14. Markwardt CB. Non-linear least squares fitting in IDL with MPFIT. In Proceedings of the astronomical data analysis software and systems XVIII, eds.Bohlender D., Dowler P., Durand D.. Quebec, Canada 2008 p. 411:251–4.
15. Koumenis C, Wouters BG. "Translating" tumor hypoxia: unfolded protein response (UPR)-dependent and UPR-independent pathways. Mol Cancer Res 2006;4:423–36.
16. Lando M, Holden M, Bergersen LC, Svendsrud DH, Stokke T, Sundfor K, et al. Gene dosage, expression, and ontology analysis identifies driver genes in the carcinogenesis and chemoradioresistance of cervical cancer. PLoS Genet 2009;5:e1000719.
17. Beisvag V, Junge FK, Bergum H, Jolsum L, Lydersen S, Gunther CC, et al. GeneTools–application for functional annotation and statistical hypothesis testing. BMC Bioinformatics 2006;7:470.

18. Dinu I, Potter JD, Mueller T, Liu Q, Adewale AJ, Jhangri GS, et al. Improving gene set analysis of microarray data by SAM-GS. BMC Bioinformatics 2007;8:242.
19. Amundson SA, Do KT, Vinikoor LC, Lee RA, Koch-Paiz CA, Ahn J, et al. Integrating global gene expression and radiation survival parameters across the 60 cell lines of the National Cancer Institute Anticancer Drug Screen. Cancer Res 2008;68:415–24.
20. Chiang DY, Villanueva A, Hoshida Y, Peix J, Newell P, Minguez B, et al. Focal gains of VEGFA and molecular classification of hepatocellular carcinoma. Cancer Res 2008;68:6779–88.
21. Ishigami T, Uzawa K, Higo M, Nomura H, Saito K, Kato Y, et al. Genes and molecular pathways related to radioresistance of oral squamous cell carcinoma cells. Int J Cancer 2007;120:2262–70.
22. Mense SM, Sengupta A, Zhou M, Lan C, Bentsman G, Volsky DJ, et al. Gene expression profiling reveals the profound upregulation of hypoxia-responsive genes in primary human astrocytes. Physiol Genomics 2006;25:435–49.
23. Starmans MH, Krishnapuram B, Steck H, Horlings H, Nuyten DS, van de Vijver MJ, et al. Robust prognostic value of a knowledge-based proliferation signature across large patient microarray studies spanning different cancer types. Br J Cancer 2008;99:1884–90.
24. Winter SC, Buffa FM, Silva P, Miller C, Valentine HR, Turley H, et al. Relation of a hypoxia metagene derived from head and neck cancer to prognosis of multiple cancers. Cancer Res 2007;67:3441–9.
25. Olcina M, Lecane PS, Hammond EM. Targeting hypoxic cells through the DNA damage response. Clin Cancer Res 2010;16:5624–9.
26. Chi JT, Wang Z, Nuyten DS, Rodriguez EH, Schaner ME, Salim A, et al. Gene expression programs in response to hypoxia: cell type specificity and prognostic significance in human cancers. PLoS Med 2006;3:e47.
27. Law AY, Wong CK. Stanniocalcin-2 is a HIF-1 target gene that promotes cell proliferation in hypoxia. Exp Cell Res 2010;316:466–76.
28. Hamaguchi T, Iizuka N, Tsunedomi R, Hamamoto Y, Miyamoto T, Iida M, et al. Glycolysis module activated by hypoxia-inducible factor 1α is related to the aggressive phenotype of hepatocellular carcinoma. Int J Oncol 2008;33:725–31.
29. Lee PJ, Jiang BH, Chin BY, Iyer NV, Alam J, Semenza GL, et al. Hypoxia-inducible factor-1 mediates transcriptional activation of the heme oxygenase-1 gene in response to hypoxia. J Biol Chem 1997;272:5375–81.
30. Burkart A, Shi X, Chouinard M, Corvera S. Adenylate kinase 2 links mitochondrial energy metabolism to the induction of the unfolded protein response. J Biol Chem 2011;286:4081–9.
31. Ito D, Walker JR, Thompson CS, Moroz I, Lin W, Veselits ML, et al. Characterization of stanniocalcin 2, a novel target of the mammalian unfolded protein response with cytoprotective properties. Mol Cell Biol 2004;24:9456–69.
32. Wouters BG, Koritzinsky M. Hypoxia signalling through mTOR and the unfolded protein response in cancer. Nat Rev Cancer 2008;8:851–64.
33. Fyles A, Milosevic M, Hedley D, Pintilie M, Levin W, Manchul L, et al. Tumor hypoxia has independent predictor impact only in patients with node-negative cervix cancer. J Clin Oncol 2002;20:680–7.
34. Feldman DE, Chauhan V, Koong AC. The unfolded protein response: a novel component of the hypoxic stress response in tumors. Mol Cancer Res 2005;3:597–605.
35. Hofbauer KH, Gess B, Lohaus C, Meyer HE, Katschinski D, Kurtz A. Oxygen tension regulates the expression of a group of procollagen hydroxylases. Eur J Biochem 2003;270:4515–22.
36. Schodel J, Oikonomopoulos S, Ragoussis J, Pugh CW, Ratcliffe PJ, Mole DR. High-resolution genome-wide mapping of HIF-binding sites by ChIP-seq. Blood 2011;117:e207-e217.
37. Ewing RM, Chu P, Elisma F, Li H, Taylor P, Climie S, et al. Large-scale mapping of human protein-protein interactions by mass spectrometry. Mol Syst Biol 2007;3:89.
38. Gess B, Hofbauer KH, Wenger RH, Lohaus C, Meyer HE, Kurtz A. The cellular oxygen tension regulates expression of the endoplasmic oxidoreductase ERO1-Lalpha. Eur J Biochem 2003;270:2228–35.
39. Meyer HA, Tolle A, Jung M, Fritzsche FR, Haendler B, Kristiansen I, et al. Identification of stanniocalcin 2 as prognostic marker in renal cell carcinoma. Eur Urol 2009;55:669–78.
40. Li Y, Su J, DingZhang X, Zhang J, Yoshimoto M, Liu S, et al. PTEN deletion and heme oxygenase-1 overexpression cooperate in prostate cancer progression and are associated with adverse clinical outcome. J Pathol 2011;224:90–100.
41. Goidts V, Bageritz J, Puccio L, Nakata S, Zapatka M, Barbus S, et al. RNAi screening in glioma stem-like cells identifies PFKFB4 as a key molecule important for cancer cell survival. Oncogene 2012;31:3235–43.
42. Boone B, Van GM, Lambert J, Haspeslagh M, Brochez L. The role of RhoC in growth and metastatic capacity of melanoma. J Cutan Pathol 2009;36:629–36.
43. Jamieson NB, Carter CR, McKay CJ, Oien KA. Tissue biomarkers for prognosis in pancreatic ductal adenocarcinoma: a systematic review and meta-analysis. Clin Cancer Res 2011;17:3316–31.
44. Bektas N, Noetzel E, Veeck J, Press MF, Kristiansen G, Naami A, et al. The ubiquitin-like molecule interferon-stimulated gene 15 (ISG15) is a potential prognostic marker in human breast cancer. Breast Cancer Res 2008;10:R58.
45. Cao WM, Murao K, Imachi H, Yu X, Abe H, Yamauchi A, et al. A mutant high-density lipoprotein receptor inhibits proliferation of human breast cancer cells. Cancer Res 2004;64:1515–21.
46. Kakunaga S, Ikeda W, Shingai T, Fujito T, Yamada A, Minami Y, et al. Enhancement of serum- and platelet-derived growth factor-induced cell proliferation by Necl-5/Tage4/poliovirus receptor/CD155 through the Ras-Raf-MEK-ERK signaling. J Biol Chem 2004;279:36419–25.
47. Kim JH, You KR, Kim IH, Cho BH, Kim CY, Kim DG. Over-expression of the ribosomal protein L36a gene is associated with cellular proliferation in hepatocellular carcinoma. Hepatology 2004;39:129–38.
48. Liu R, Strom AL, Zhai J, Gal J, Bao S, Gong W, et al. Enzymatically inactive adenylate kinase 4 interacts with mitochondrial ADP/ATP translocase. Int J Biochem Cell Biol 2009;41:1371–80.
49. Rouschop KM, van den Beucken T, Dubois L, Niessen H, Bussink J, Savelkouls K, et al. The unfolded protein response protects human tumor cells during hypoxia through regulation of the autophagy genes MAP1LC3B and ATG5. J Clin Invest 2010;120:127–41.
50. Law AY, Wong CK. Stanniocalcin-2 promotes epithelial-mesenchymal transition and invasiveness in hypoxic human ovarian cancer cells. Exp Cell Res 2010;316:3425–34.